© 2017. Published by The Company of Biologists Ltd | Journal of Cell Science (2017) 130, 164-176 doi:10.1242/jcs.187419

SPECIAL ISSUE: 3D CELL BIOLOGY

RESEARCH ARTICLE

The cytostome–cytopharynx complex of *Trypanosoma cruzi* epimastigotes disassembles during cell division

Carolina de L. Alcantara[1,2], Juliana C. Vidal[1,2], Wanderley de Souza[1,2] and Narcisa L. Cunha-e-Silva[1,2,*]

ABSTRACT

The cytostome–cytopharynx complex is the main site for endocytosis in epimastigotes of *Trypanosoma cruzi*. It consists of an opening at the plasma membrane surface – the cytostome – followed by a membrane invagination – the cytopharynx. In G1/S cells, this structure is associated with two specific sets of microtubules, a quartet and a triplet. Here, we used electron microscopy and electron tomography to build 3D models of the complex at different stages of the cell cycle. The cytostome–cytopharynx is absent in late G2 and M phase cells, whereas early G2 cells have either a short cytopharynx or no visible complex, with numerous vesicles aligned to the cytostome–cytopharynx microtubules. The microtubule quartet remains visible throughout cell division (albeit in a shorter form), and is duplicated during G2/M. In contrast, the microtubule triplet is absent during late G2/M. Cells in cytokinesis have an invagination of the flagellar pocket membrane likely to represent early stages in cytostome–cytopharynx assembly. Cells in late cytokinesis have two fully developed cytostome–cytopharynx complexes. Our data suggest that the microtubule quartet serves as a guide for new cytostome–cytopharynx assembly.

KEY WORDS: Cytostome, *Trypanosoma cruzi*, Tridimensional reconstruction, Cell cycle

INTRODUCTION

The cytostome–cytopharynx complex is a specialized structure found in the proliferative stages of the protozoan parasite *Trypanosoma cruzi*, the causative agent of Chagas disease. In epimastigotes, the proliferative form found in the insect vector, the cytostome–cytopharynx is the major site for endocytosis (Porto-Carreiro et al., 2000), rather than the 'flagellar pocket', which represents the sole site for endocytosis and exocytosis in other human pathogens from the same family (the Trypanosomatidae), such as *Trypanosoma brucei* and *Leishmania sp.* (Webster and Russell, 1993).

The cytostome–cytopharynx complex consists of an opening at the plasma membrane surface, close to the flagellar pocket, called the 'cytostome', followed by a deep membrane invagination, called the 'cytopharynx'. In a previous work, we have used 3D reconstruction by electron tomography to examine the structure of the cytostome–cytopharynx in detail, and showed that seven microtubules follow the path of the cytopharynx (Alcantara et al., 2014). These microtubules are arranged as a triplet that runs from underneath the cytostome membrane to the posterior of the cell, and four microtubules that run from staggered positions underneath the flagellar pocket membrane to the cytopharynx, following the path of the preoral ridge, a specialized membrane domain found between the flagellar pocket opening and the cytostome. Our tomography data show that the cytopharynx microtubule quartet is clearly distinct from the microtubule quartet typically associated with the flagellum attachment zone in trypanosomatids (this latter quartet is denoted MtQ) (Taylor and Godfrey, 1969; Vickerman, 1969; Lacomble et al., 2009). These cytostome–cytopharynx microtubules accompany the cytopharynx along its path, in a typical 'gutter' arrangement that leaves a microtubule-free side on the cytostome membrane, where vesicles can bud or fuse, during endocytosis.

During cell division, duplication of the cytostome–cytopharynx complex must be coordinated with the complex pattern of organelle and cytoskeletal remodeling characteristic of trypanosomatid cell division (Sherwin and Gull, 1989; De Souza, 2002; Vaughan and Gull, 2008). This pattern is required to faithfully duplicate and segregate a number of single-copy organelles, including the mitochondrion, the kinetoplast (the region of the mitochondrion containing the DNA, known as kDNA), the basal body complex and the flagellum. In *T. cruzi* epimastigotes the G1 phase of the cell cycle lasts for approximately 10 h, and is followed by an S phase where both mitochondrial (kinetoplast) and nuclear DNA genomes replicate (Elias et al., 2007). In the G2 phase, which lasts ∼8.6 h, the pro-basal body matures and elongates into a new flagellum, which emerges from the flagellar pocket next to the old flagellum, at the anterior region of the cell. G2 is also characterized by kinetoplast segregation and flagellar pocket duplication. A short M phase (∼0.4 h) then follows, in the absence of nuclear envelope disassembly (i.e. a 'closed' mitosis), and the daughter cells eventually separate by cytokinesis, which proceeds from a cleavage furrow that initiates at the anterior end of the cell and then proceeds toward the posterior end.

During cell division, duplication of the site of endocytosis – the flagellar pocket – has been described in detail by tomography-based 3D reconstruction in *T. brucei* (Lacomble et al., 2010). In this parasite, flagellar pocket duplication is a semi-conservative process that starts with the formation of a membrane ridge inside the single flagellar pocket of early division cells. Similar to the cytostome–cytopharynx, the flagellar pocket is a specialized cell membrane domain devoid of subpellicular microtubules, but associated with a specialized set of microtubules – the MtQ – which duplicate early in cell division, before probasal body maturation and elongation, in a position anterior to the old MtQ. In *T. cruzi*, however, comparatively little is known about organelle and cytoskeleton duplication during cell division (Elias et al., 2007; Ramos et al., 2011), and the events involved in the division and segregation of the cytostome–cytopharynx complex have not been described. In our previous work (Alcantara et al., 2014), we showed that the cytopharynx of cells in early G2 (i.e. with a short new flagellum, a single nucleus

[1]Instituto de Biofísica Carlos Chagas Filho, Universidade Federal do Rio de Janeiro, Rio de Janeiro 21941-902, Brazil. [2]Núcleo de Biologia Estrutural e Bioimagens (CENABIO), Rio de Janeiro 21941-902, Brazil.

*Author for correspondence (narcisa@biof.ufrj.br)

N.L.C., 0000-0003-4863-4945

Received 4 February 2016; Accepted 27 June 2016

Journal of Cell Science (2017) 130, 164-176 doi:10.1242/jcs.187419

and a single kinetoplast) is longer and appears less helical than that of cells in G1/S, although it retains its endocytic capacity. However, we did not analyze this structure at later stages of the cell cycle, to elucidate its duplication pattern.

Here, we investigate the duplication of the epimastigote cytostome–cytopharynx complex in detail, using advanced methods of cellular 3D reconstruction-including focused ion beam scanning electron microscopy (FIB-SEM) and electron microscopy tomography applied to the analysis of populations of synchronized cells.

RESULTS

T. cruzi epimastigotes in the early G2 phase of the cell cycle, characterized by the presence of one nucleus, one kinetoplast and two flagella (1N1K2F), still possess a single cytostome–cytopharynx complex (Ramos et al., 2011) and, despite a relatively discrete morphological change in shape and length, this complex remains functional, being able to uptake endocytic tracers (Alcantara et al., 2014). Later stages of the cell cycle (mitosis and cytokinesis) are of short duration (Elias et al., 2007), which makes the analysis of cells in these key cell cycle phases difficult in non-synchronized cultures. Therefore, to study the biogenesis of the cytostome–cytopharynx complex during cell division, we arrested cells in the G1 phase of the cell cycle by using hydroxyurea (HU) and analyzed cell populations 10–14 h after release from the HU block, where cells in G2, mitosis and cytokinesis are more abundant (Galanti et al., 1994; Elias et al., 2007). At 1 h after HU removal, 91% of the cells were in G1 (Fig. S1A) as accessed by observation and counting of cells using phase contrast and DAPI staining at an optical microscope. We established that the 11 h post-HU block release (Fig. S1A), which was the earliest time point where a higher proportion of cells at later stages in the cell cycle (end of G2, mitosis and cytokinesis) were found, represented the ideal time-point for analysis of cytostome–cytopharynx duplication.

The cytostome–cytopharynx complex is a large structure (6–11 µm in length; Alcantara et al., 2014) that extends from the anterior region of the cell to the posterior. Thus, to evaluate the architecture of the whole complex in dividing cells, we used FIB-SEM, a powerful technique for 3D reconstruction by electron microscopy that allows the imaging of a large number of cells in their entirety in a single image series (Alcantara et al., 2014; Kizilyaprak et al., 2014). Although FIB-SEM is an ideal technique to analyze the overall 3D architecture of cellular components, it has relatively limited resolution (up to 10 nm) compared with conventional thin-section TEM (resolution of up to 1 nm). Thus, we combined the findings using FIB-SEM with serial electron tomography data, to improve the resolution of specific events in the cycle of cytostome–cytopharynx duplication. See Table S1 for a summary of the number of cells analyzed in each cell cycle stage by FIB-SEM and electron tomography.

The cytopharynx disappears during early G2 phase

Using FIB-SEM, we analyzed the morphology of the cytostome–cytopharynx complex in cells in different stages of G2. In epimastigotes in early G2 whose kinetoplast had not yet started dividing but where the new flagellum had already exited the flagellar pocket, the cytopharynx was shorter in length, having a mean length of 4.4 µm (Fig. 1A–F). The arrangement and number of accompanying microtubules and vesicles did not appear altered relative to that observed in cells in G1/S (Fig. 1C,D,F; Alcantara et al., 2014), with quartet and triplet microtubules possessing their typical helical format, and extending from the cytostome to the posterior of the cell, past the end of the cytopharynx (Fig. 1F).

Striking cytostome–cytopharynx modifications were clear at a slightly later stage in G2 (Fig. 1G–I; Fig. 2), in cells with a dividing kinetoplast, described as a disk with a central hole found in early kinetoplast segregation (Ferguson et al., 1994; Ramos et al., 2011; Jensen and Englund, 2012). In some cells at this stage, the cytostome opening, whose mean diameter is ∼100 nm (Vatarunakamura et al., 2005), was smaller than that observed in G1, measuring only 46 nm (Fig. 1G) and the cytopharynx was short, measuring only 0.6 µm in length (Fig. 1H,I).

In other cells at the same stage in the cell cycle (judging from kinetoplast morphology), the cytostome–cytopharynx complex was absent (Fig. 2; Movie 1). A microtubule quartet likely corresponding to that of the cytopharynx ran past the flagellar pocket opening (Fig. 2A) towards the expected position of the cytostome, but the cytostome opening was not clear. The quartet then bent towards the interior of the cell (Fig. 2B–E), together with the microtubule triplet that started underneath the cytostome (see Movie 1), following the expected path of the cytopharynx towards the posterior. However, no cytopharynx was visible; instead, many vesicles were aligned to these microtubules (Fig. 2C-F), which extended until the post-nuclear region (Fig. 2F). These vesicles were similar in morphology and diameter to those observed lining the cytopharynx in cells in G1 (Alcantara et al., 2014). The preoral ridge, a differentiated membrane domain located between the flagellar pocket and the cytostome (De Souza et al., 1978; Vatarunakamura et al., 2005; Guedes et al., 2012) was also absent (data not shown). In total, the cytostome–cytopharynx complex was absent in nine cells at this stage (from different biological replicates, Table S1), which suggests that the complex disassembles during kinetoplast segregation, before the complete formation of two separate kinetoplast masses.

Interestingly, cells with a very short or absent cytopharynx had either one or two Golgi complexes (compare Fig. 1H,I with Fig. 2C,D,F), suggesting that the disassembly of the cytopharynx during the cell cycle was also concomitant with Golgi duplication.

The disassembly of the main endocytic portal prompted us to analyze the endocytic capacity of epimastigotes in the different cell cycle stages (Fig. S1B). At 11 h post HU removal, we incubated the cells with transferrin coupled to the fluorescein isothiocyanate (Tf–FITC) for 15 min at 28°C. Washed and fixed parasites were analyzed under the fluorescence microscope to determine the cell cycle stage and the presence of the endocytic tracer. We observed that 17.3% of cells in early G2 (1N1K2F) did not endocytose Tf-FITC. This proportion is only slightly higher than the proportion of cells in G1 that did not endocytose. Moreover, 97% of the cells that had already duplicated the kinetoplast (1N2K2F) did not endocytose Tf–FITC (Fig. S1B, C1,2). Surprisingly, the endocytic capacity was rapidly recovered, as only 31.1% of the cells in cytokinesis (2N2K2F) were still incapable of uptake of the tracer (Fig, S1B,C3,4). Note that the tracer was found at the anterior region of the cell body in twice the number of these parasites compared with G1 parasites. Cells at the end of cytokinesis, with two nuclei, two kinetoplasts and the two flagella that were opposed to each other (Fig. S1C5,6), already presented the tracer. These data show that the endocytic activity is markedly reduced during a short period of the cell cycle, ranging from late G2 to the beginning of cytokinesis.

The cytostome–cytopharynx complex is absent in cells with two kinetoplasts and two flagellar pockets

In *T. cruzi* epimastigotes, the presence of two kinetoplasts and two flagellar pockets are hallmarks of the late G2 phase of cell cycle, immediately prior to mitosis (Elias et al., 2007). Cells at this stage did not have a cytostome–cytopharynx complex (Fig. 3; Movie 2),

Journal of Cell Science (2017) 130, 164-176 doi:10.1242/jcs.187419

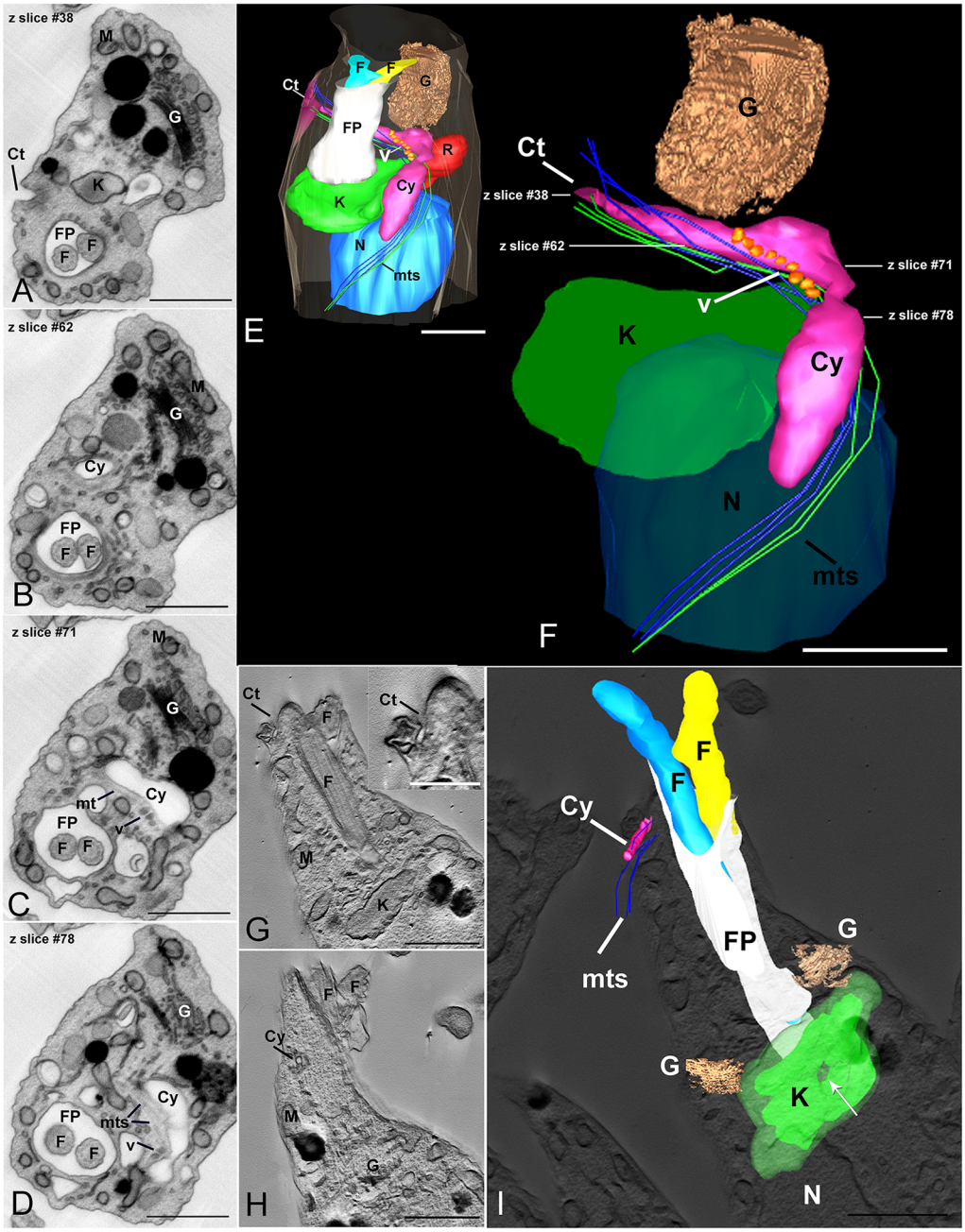

Fig. 1. Morphological changes of the cytostome–cytopharynx complex during G2. *Trypanosoma cruzi* epimastigotes were fixed and processed for electron microscopy 11 h after release from HU block (for G1 arrest), and imaged by FIB-SEM microscopy (A–F) and serial tomography (G–I). (A–D) Sequence of images of a cell in early G2 phase (1N1K2F) showing different portions of the cytostome–cytopharynx complex. (E,F) 3D models show the positioning of the cytostome (Ct)–cytopharynx (Cy) complex (in pink) in the context of other cell structures, including the nucleus (N, in blue), the kinetoplast (K, in green), the flagellar pocket (FP, in white), the two flagella (F1 and F2, in yellow and light blue, respectively), the Golgi complex (Gc, in gold), the reservosomes (R, in red), as well as the cytopharynx-associated microtubules (mts; blue and green tubes, for the cytopharynx microtubule quartet and triplet, respectively) and vesicles (v, in orange). The cytostome is located at the anterior region of the cell, close to the flagellar pocket opening (A,E). Towards the posterior of the cell, the lumen of the cytopharynx is enlarged and electron-lucent, with different diameters along its length (B–F). The cytopharynx is accompanied by its characteristic microtubules along its entire length, and is also lined with vesicles, ending in a tubular protrusion. Note that this cell has only one (albeit enlarged) Golgi complex, supporting the classification that it is at a very early stage in G2. Virtual slices (G–H), and 3D model (I) from a serial tomogram of an epimastigote at a slightly later cell cycle stage in G2 than the cell displayed in A–F, judging from the presence of two Golgi complexes, and of a dividing kinetoplast (as identified by the central 'gap' indicated by a white arrow in I). In the 3D model (I), a slice from the tomogram appears on the background (in dark gray), to aid in the positioning of the segmented structures relative to the cell surface. In this cell, the cytostome appears very small (inset in G), and is followed by a short cytopharynx (H) accompanied by microtubules. M, mitochondrion. Scale bars: 1 µm (A–I); 0.5 µm (inset in G).

confirming the observation that this complex is disassembled earlier in the cycle, in early G2.

In late G2, the microtubule quartet likely corresponding to that of the cytopharynx (located near the flagellar pocket from which the old flagellum emerges) was shorter. Similarly to that observed in G1 cells, this quartet exhibited a bend towards the center of the cell; however, the bend region was somewhat distant from the plasma membrane (Fig. 3A,E), rather than being positioned immediately

Journal of Cell Science (2017) 130, 164-176 doi:10.1242/jcs.187419

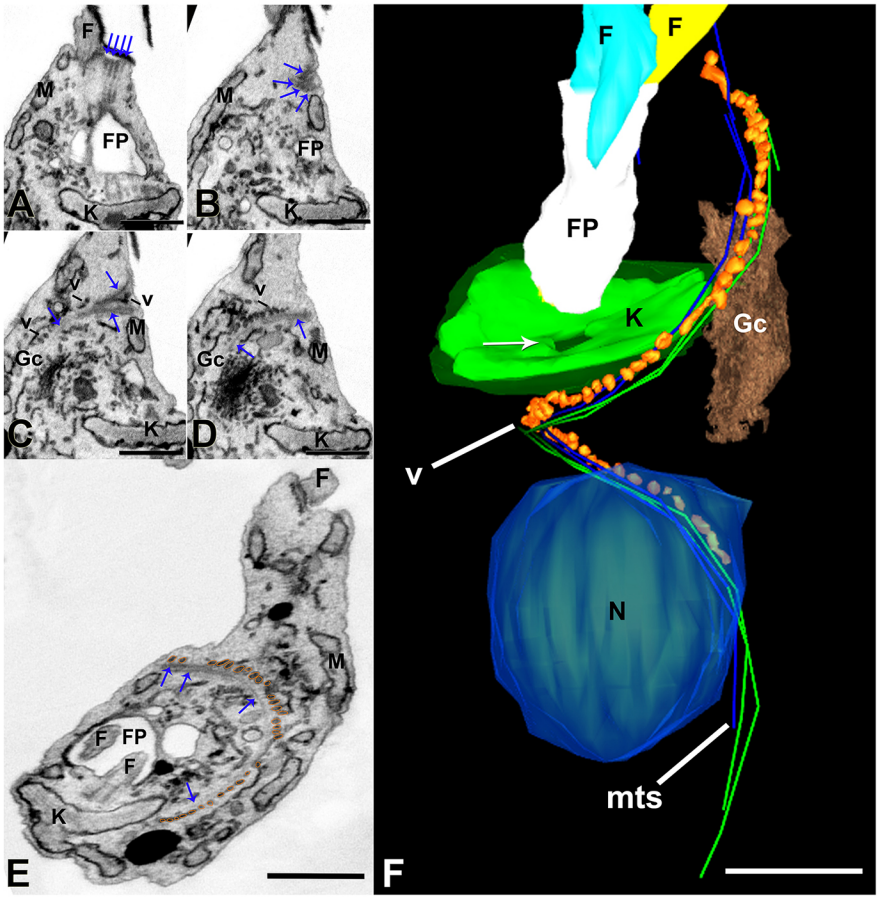

Fig. 2. Disappearance of the cytostome–cytopharynx complex during early G2. Sequential images from a FIB-SEM series of an early G2-phase *Trypanosoma cruzi* epimastigote (A–D). Rotated view (E) and 3D reconstruction (F) of the same cell. (A) From the anterior of the cell, near the flagellar pocket (FP, in white), four microtubules (blue arrows) can be identified. (B–F) These microtubules (mts, pointed by the blue arrows or represented as blue and green tubes in the reconstruction in F) runs towards the center of the cell, following the expected path of the cytostome–cytopharynx complex; however, the cytopharynx itself could not be seen, and the cytostome was not conspicuous (possibly due to the absence of the cytopharynx lumen to 'mark' the cytostome opening). Along most of their path – which goes deep into the cytoplasm, past the Golgi complex (Gc, in gold) and the nucleus (N, in blue) – these microtubules appeared to be associated with numerous aligned vesicles (v in C,D and orange in E, F). This cell has only one Golgi complex and a dividing kinetoplast (K, green), identified by the presence of a central gap in the structure (white arrow in F). Flagellum (F, yellow and light blue). M, mitochondrion. Scale bars: 1 µm. The complete imaging, by FIB-SEM, of the cell shown here can be found in Movie 1.

below the membrane, as observed in G1 cells (Fig. 3A–C,G–I). Adjacent to the flagellar pocket of the new flagellum, we also observed four short microtubules underneath the flagellar pocket membrane (Fig. 3D–I). These microtubules displayed the same arrangement as the ones near the flagellar pocket of the old flagellum, bending towards the center of the cell, and always close to the Golgi complex (Fig. 3G–I). The microtubule triplet of the cytopharynx appeared absent at this cell cycle stage, as we were unable to visualize or track them in any cell at this stage, even using electron tomography, which can give a better resolution for the observation of this feature.

The microtubule quartet associated with each duplicated flagellar pocket remains short during M phase

In cells undergoing mitosis, we did not observe any structures resembling a cytostome–cytopharynx complex, and no triplet microtubules were visible (Fig. 4). In addition, each of the duplicated flagellar pockets of cells at this stage was associated with a short microtubule quartet (Fig. 4A–K; Movie 3). As in the previous cell cycle stage, this quartet of microtubules was found underlying the flagellar pocket membrane and then bending towards the Golgi complex, not reaching the flagellar pocket opening region (Fig. 4J,K). To improve microtubule identification in these cells, we also imaged a mitotic cell using serial electron tomography (Fig. 4L,M). A detailed view of one of the flagellar pockets of this cell (Fig. 4M) showed that the set of four microtubules lining the flagellar pocket membrane and then bending towards the center of the cell was clearly distinct from the conserved flagellar pocket MtQ, which was located closely apposed to the flagellar pocket membrane. Thus, the short microtubule quartet associated with each of the duplicated flagellar pockets most likely represents the one that follows the path of the cytostome–cytopharynx complex in G1/S cells. As a reference to its location in the G1 cell, this quartet will be, henceforth, referred to as the cytopharynx microtubule quartet in cells at all cell cycle stages, even though in some cell cycle stages the cytopharynx itself appears to be absent.

To rule out that the disappearance of the cytostome–cytopharynx invagination and the shortening of the cytopharynx microtubule quartet might result from the HU treatment, we also imaged untreated cells in mitosis (Fig. S2). In the mitotic cell depicted in Fig. S2A,B, both flagellar pockets (Fig. S2C,D) were associated with a microtubule quartet that was aligned with the flagellar pocket membrane before bending towards the cell cytoplasm close to the Golgi complex. These microtubules likely correspond to the cytopharynx microtubule quartet, because we could observe, in the same plane, the flagellar pocket MtQ in a different orientation, closely apposed to the flagellar pocket membrane (Fig. S2C).

New cytostome–cytopharynx complexes are formed from the flagellar pocket membrane during cytokinesis

In cells at the beginning of cytokinesis, which exhibited a characteristic 'heart' shape, a rudimentary cytopharynx started to assemble from the flagellar pocket membrane (Figs 5 and 6). In a serial tomogram covering the area around one of the flagellar pockets in a cell in early cytokinesis (Fig. 5A,B), both the conserved MtQ of the flagellar pocket and the cytopharynx microtubule quartet (indicated by blue arrows in Fig. 5) were visible. Close to the flagellar pocket opening, the membrane displayed a discrete invagination that was associated with the cytostome–cytopharynx cytoskeleton, including both the cytopharynx microtubule quartet (blue arrows) and

Journal of Cell Science (2017) 130, 164-176 doi:10.1242/jcs.187419

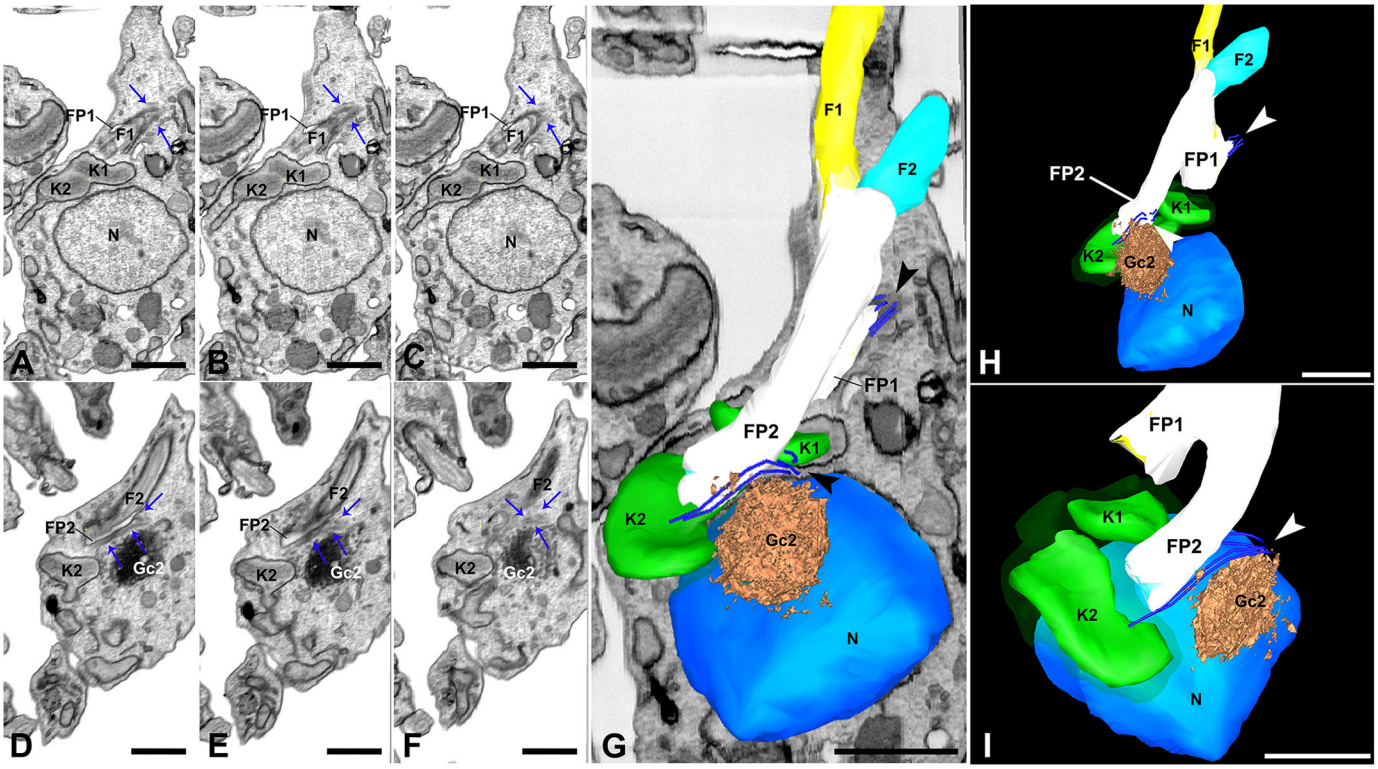

Fig. 3. Shortening of the cytopharynx microtubule quartet is concomitant with quartet duplication, in late G2. FIB-SEM images (A–F) and corresponding 3D model (G–I) of a *Trypanosoma cruzi* epimastigote in the late G2 stage of the cell cycle. The cell possesses one nucleus (N, in blue), a dividing kinetoplast with two separated kDNA masses (K1 and K2, in green), two individualized flagellar pockets (FP1 and FP2, in white) and two flagella (F1 and F2, in yellow and light blue, respectively). (A–C) Close to the membrane of the flagellar pocket (FP1) from which the old flagellum (F1) emerges, a microtubule quartet (blue arrows in A–C, and blue tubes in G–I) projects towards the cytoplasm. This quartet likely corresponds to that associated with the cytopharynx in G1/S cells, and is considerably shorter than that observed in early G2 cells. (D–F) Adjacent to the flagellar pocket (FP2) from which the new flagellum (F2) emerges, a new cytopharynx microtubule quartet (blue arrows in D–F, and blue tubes in G–I) is also visible near the flagellar pocket membrane, and extends by a short length towards the cytoplasm, passing very close to the nearby Golgi complex (Gc2). No cytopharynx was visible in this cell. We could not identify, in late G2 cells, a microtubule triplet that could correspond to the one associated with the cytostome–cytopharynx of G1/S cells. The arrowhead in G–I indicates the cytopharynx microtubule quartet. Scale bars: 1 µm. The complete imaging, by FIB-SEM, of the cell shown here can be found in Movie 2.

the triplet (green arrows; Fig. 5D,E). Although the invagination was shallow, the two microtubule sets associated with it followed a path identical to that of the cytopharynx microtubules in G1/S cells (Alcantara et al., 2014), extending further towards the center of the cell, and passing very close to the Golgi complex (Fig. 5F,G). We identified two additional cytoplasmic microtubules (named 1 and 2 in Fig. 5H and I, respectively) in this serial tomogram. One end of these microtubules was located near the cytopharynx microtubule quartet, in the region where this quartet underlies the flagellar pocket membrane. Then, these individual microtubules ran past opposites sides of the Golgi complex, extending towards the center of the cell (Fig. 5J).

FIB-SEM imaging allowed the visualization of both flagellar pocket areas of cells in cytokinesis (Fig. 6), and confirmed the serial tomogram data, showed in Fig. 5, that flagellar pockets of cells at this stage often contain an invagination associated with the cytopharynx cytoskeleton. This short invagination is apparent in the flagellar pocket of daughter cell 2 in Fig. 6, and is surrounded by the two sets of cytopharynx microtubules (the triplet, indicated by green arrows, and the quartet, indicated by blue arrows). While the invagination itself was short and did not reach the Golgi complex (Fig. 6K), the microtubules extended further towards the cell posterior. The 3D model (Fig. 6N) shows that the microtubules surrounding the flagellar pocket invagination assume the ‘gutter’ arrangement typically observed in the cytostome–cytopharynx complex found in cells at earlier stages of the cell cycle (Alcantara et al., 2014). Although no invagination was apparent in the flagellar pocket of daughter cell 1, the quartet and triplet microtubules found next to each other in the flagellar pocket region extended towards the posterior of the cell, close to the reservosomes (Fig. 6G), also assuming the characteristic ‘gutter’ arrangement (Fig. 6E). Only two microtubules from each set reached the posterior of the cell (Fig. 6G). The same process was observed in parasites that had not been synchronized with HU (control cells) at this cell cycle stage (Fig. S3).

FIB-SEM imaging of cells at a later stage in cytokinesis (Fig. 7; Movie 4) confirmed that the flagellar pocket invagination observed in cells in early cytokinesis corresponds to a new cytopharynx. The FIB-SEM series of the cells shown covered the entire region of the flagellar pocket up to the post-nuclear region in daughter cell 1 (the one on the left in Fig. 7A,F) and just the post-nuclear region of daughter cell 2 (the one on the right in Fig. 7A,F). The flagellar pocket of daughter cell 1 contains a membrane invagination that is accompanied by the cytopharynx microtubules (blue arrows in Fig. 7B,C). This invagination, with a total length of 2.1 µm, runs deep into the cytoplasm and is associated with cytopharynx microtubules (Fig. 7D,E,G). Rotation of the imaged volume revealed a longitudinal view of the cytopharynx, and allowed us to visualize the lumen of the structure in detail (Fig. 7I). Although the plane immediately anterior to the cytopharynx showed its associated microtubules (Fig. 7H,K), observation of a longitudinal

Journal of Cell Science (2017) 130, 164-176 doi:10.1242/jcs.187419

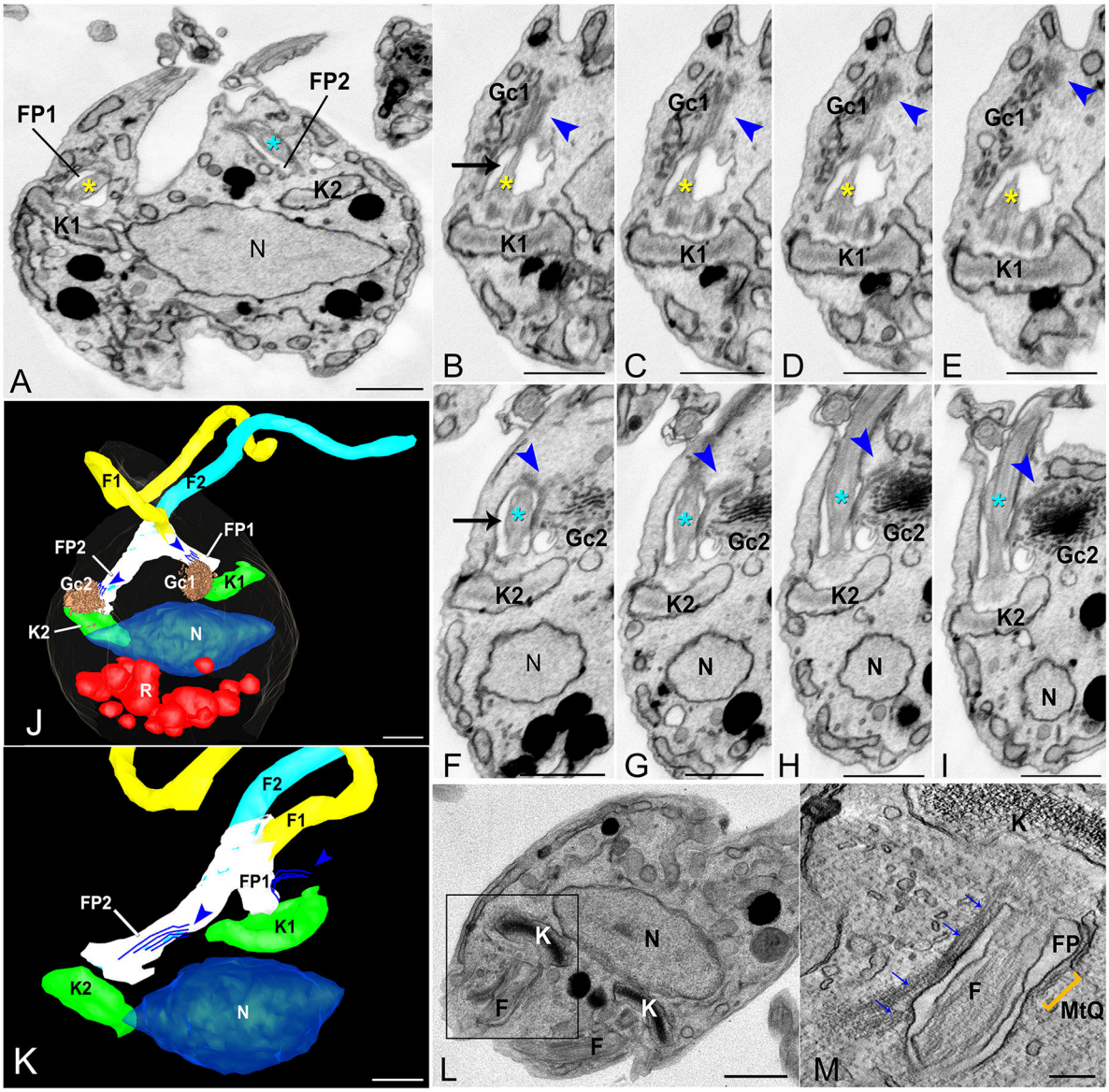

Fig. 4. The cytopharynx microtubule quartet remains short during mitosis. *Trypanosoma cruzi* epimastigotes in mitosis imaged by FIB-SEM and electron tomography. (A–K) FIB-SEM images (A–I) and corresponding 3D model (J,K) of a cell with an elongated mitotic nucleus (N, in blue), two flagellar pockets (FP1 and FP2, in white), an old and a new flagellum (F1 and F2, in yellow and light blue asterisks, respectively), two kinetoplasts (K1 and K2, in green), and two Golgi complexes (Gc1 and Gc2, in gold). Both the flagellar pocket on the left (B–E) and that on the right (F–I) (indicated by arrow in B and F) are associated with a short cytopharynx microtubule quartet (blue arrowhead) that runs from the flagellar pocket towards the nearby Golgi complex. The reservosomes (R, in red) found at the posterior of the cell were also included in the model. (L) 0° image of a serial tomogram of a different epimastigote in mitosis, showing one of the flagellar pocket regions in higher resolution. (M) Magnification of the area indicated by the rectangle in L. In this tomogram the cytopharynx microtubule quartet (blue arrows) can be clearly distinguished from the classical MtQ of the flagellar pocket (orange brackets). Scale bars: 1 µm (A,J,K,L); 500 nm (B–I); 200 nm (M). The complete imaging, by FIB-SEM, of the cell shown here can be found in Movie 3.

plane in the middle of the structure (Fig. 7I) displayed an electron-lucent lumen with an electron-dense internal membrane coat (arrowhead) indistinguishable from that observed in the cytopharynx of G1/S cells (Cunha-e-Silva et al., 2010; Alcantara et al., 2014). In a plane immediately adjacent to that of the cytopharynx lumen (and opposite to that containing the 'gutter' of microtubules), many vesicles with electron-dense content were aligned to the microtubule-free side of the cytopharynx membrane (Fig. 7J,L), including one vesicle in direct contact with the membrane (Fig. 7M,N).

At the end of cytokinesis, daughter cells are held together by their posterior regions only, and the kinetoplast, flagellar pocket and flagellum complexes are located at opposite ends of the dividing cell, with the two flagella pointing in opposite directions (Fig. S4). FIB-SEM images and 3D reconstruction of cells at this stage revealed that each daughter cell possesses a fully formed cytostome–cytopharynx complex, indistinguishable from that observed in G1/S cells (Alcantara et al., 2014). In addition, both daughter cells have a preoral ridge, located between the flagellar pocket opening and the cytostome.

DISCUSSION

Trypanosomatids are unicellular eukaryotes with a high degree of cellular organization and polarization. Cell division in these

Journal of Cell Science (2017) 130, 164-176 doi:10.1242/jcs.187419

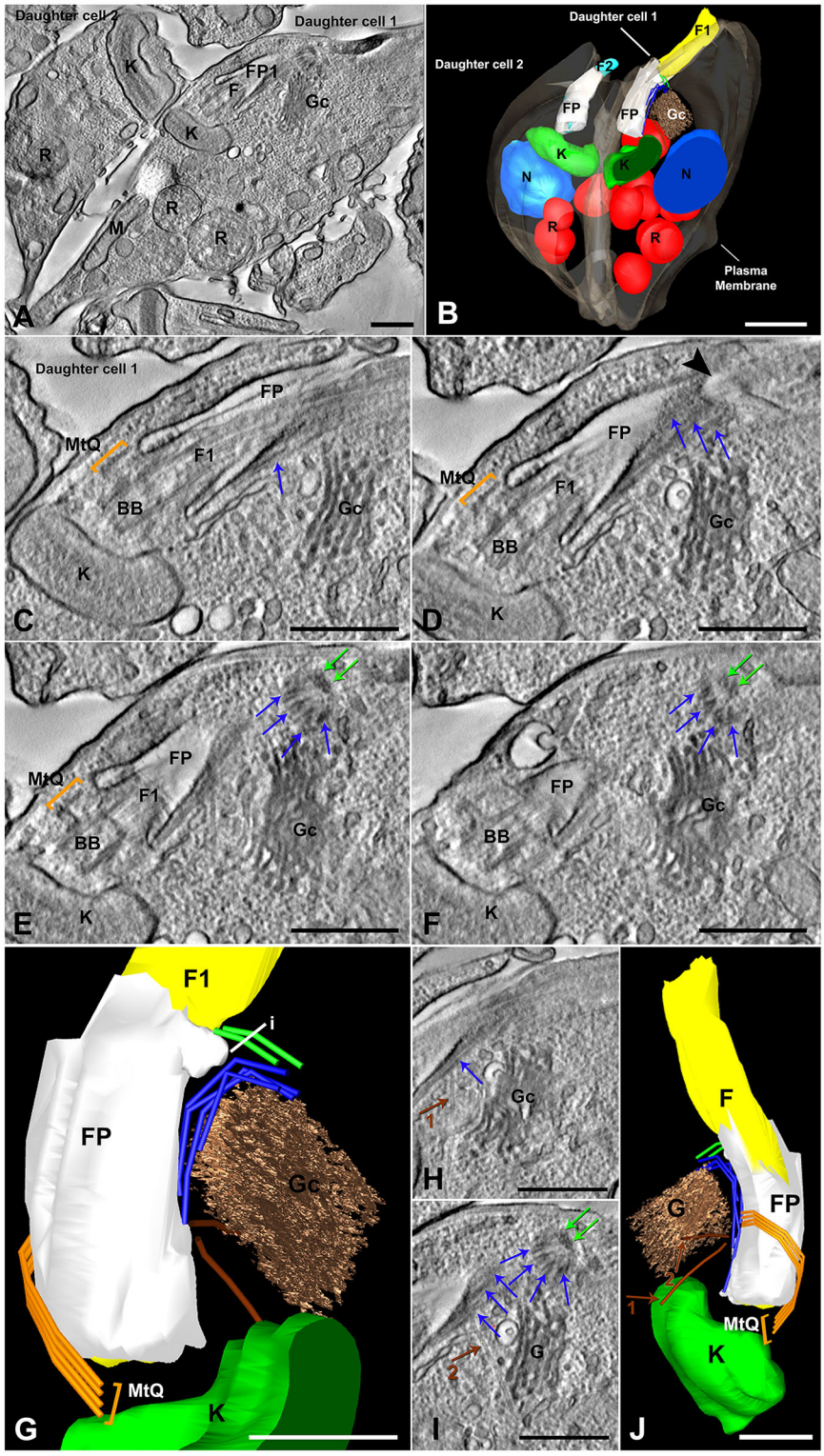

Fig. 5. At the beginning of cytokinesis, a membrane invagination is formed from the flagellar pocket and is accompanied by the cytopharynx microtubules. Serial electron tomography of an epimastigote at the beginning of the cytokinesis. Images of the tomogram (A,C–F,H,I), and corresponding 3D model (B,G,J) showing two daughter cells undergoing cytokinesis. The tomogram covered the entire volume of the flagellar pocket from daughter cell 1 (on the right, in A). K, kinetoplast (in green); FP, flagellar pocket, in white; F1 and F2, flagella (in yellow and light blue, respectively); Gc, Golgi complex, (in gold), R, reservosomes (in red); M, mitochondrion; BB, basal body. This cell displays the characteristic 'heart' shape of cells at the beginning of cytokinesis. (C–F) Sequence of images from the tomogram in the region of the flagellar pocket of daughter cell 1, showing six of the cytopharynx microtubules – four from the quartet (blue arrows) and two from the triplet (green arrows) – progressively appearing and running towards a small invagination of the flagellar pocket membrane (arrowhead in D). (E–F) The six microtubules (blue and green arrows) then bend inwards and continue towards the center of the cell, passing close to the Golgi complex. (G) A closer view of the model in the flagellar pocket region of daughter cell 1 shows the small flagellar pocket invagination (i) surrounded by the microtubules of the quartet (blue tubes) and the triplet (green tubes). Whereas the quartet of microtubules near the invagination was bent around the Golgi complex, the classical MtQ (in orange) could be seen surrounding the flagellar pocket. Two other cytoplasmic microtubules (named 1 and 2, and indicated by brown arrows in H–J) could be identified in this tomogram, extending from the cytopharynx microtubule quartet to the Golgi complex. Scale bars: 1 µm.

organisms occurs through binary fission, and typically involves the duplication of single copy organelles – including the flagellum, flagellar pocket, kinetoplast and mitochondrion, Golgi complex and nucleus – without organelle disassembly during the cell cycle. This phenomenon contrasts with the organelle and cytoskeletal disassembly and re-structuring typical of mammalian cell division (Imoto et al., 2011), and is likely to be important for the inheritance of the highly polarized trypanosomatid cell pattern, through some degree of positional guidance or templating from old structures (Sherwin and Gull, 1989; Woodward and Gull, 1990; Robinson et al., 1995). Nevertheless, we show here that the cytostome–cytopharynx complex of *T. cruzi* epimastigotes is disassembled during the cell cycle (in G2), and then formed *de novo* at each daughter cell during cytokinesis.

Although we could not identify the cytostome opening and the cytopharynx invagination in late G2 cells (Figs 2 and 3), the

Journal of Cell Science (2017) 130, 164-176 doi:10.1242/jcs.187419

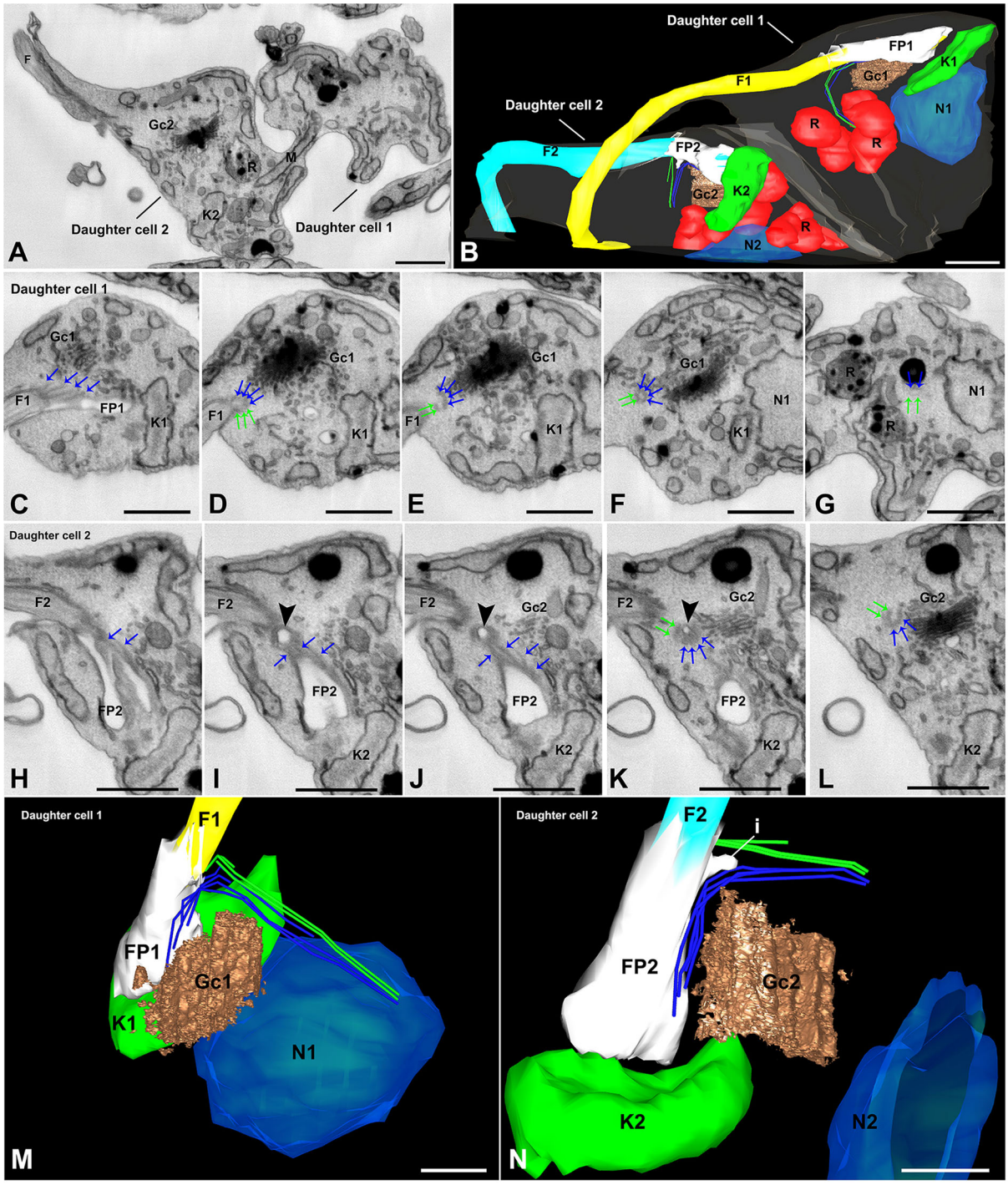

Fig. 6. Formation of new cytostome–cytopharynx complexes in daughter cells during cytokinesis. FIB-SEM images (A,C–L) and corresponding 3D model (B,M,N) of a *Trypanosoma cruzi* epimastigote in cytokinesis, showing the flagella (F1 and F2, in yellow and light blue, respectively), the flagellar pockets (FP1 and FP2, in white), the kinetoplasts (K1 and K2, in green), the nuclei (N1 and N2, in blue), the Golgi complexes (Gc1 and Gc2, in gold) and the reservosomes (R, in red). In daughter cell 1 (C–G, model in M), the cytopharynx microtubule quartet (blue arrows in images, and blue tubes in 3D model) and the triplet (green arrows in images, and green tubes in 3D model) run from the flagellar pocket region towards the nucleus, bending around the Golgi complex. Note that one of the microtubules from the triplet was very short (ended between images D and E), with only two microtubules from each set found at the posterior of the cell (G), close to the reservosomes (R). In the flagellar pocket region of daughter cell 2 (H–L, model in N), the microtubules from the quartet and the triplet converge into a 'gutter' shape, following the path of a membrane invagination (arrowhead) formed near the collar region of the flagellar pocket. The microtubules then continue past the Golgi complex, but only three of the four microtubules from the quartet could be seen at the end of the series. Scale bars: 1 µm (A–L); 0.5 µm (M,N).

cytoskeleton associated with the cytostome–cytopharynx complex did not fully disassemble during the cell cycle (Figs 2–8). In particular, the microtubule quartet that follows the cytopharynx (in G1/S cells) remained visible throughout the cell cycle, although in a shorter form, indicating that these microtubules are partially depolymerized in late G2 (Fig. 3). The quartet is duplicated in G2 and then elongates in cytokinesis, returning to its original size. Interestingly, elongation of the microtubule quartet towards the posterior during cytokinesis

Journal of Cell Science (2017) 130, 164-176 doi:10.1242/jcs.187419

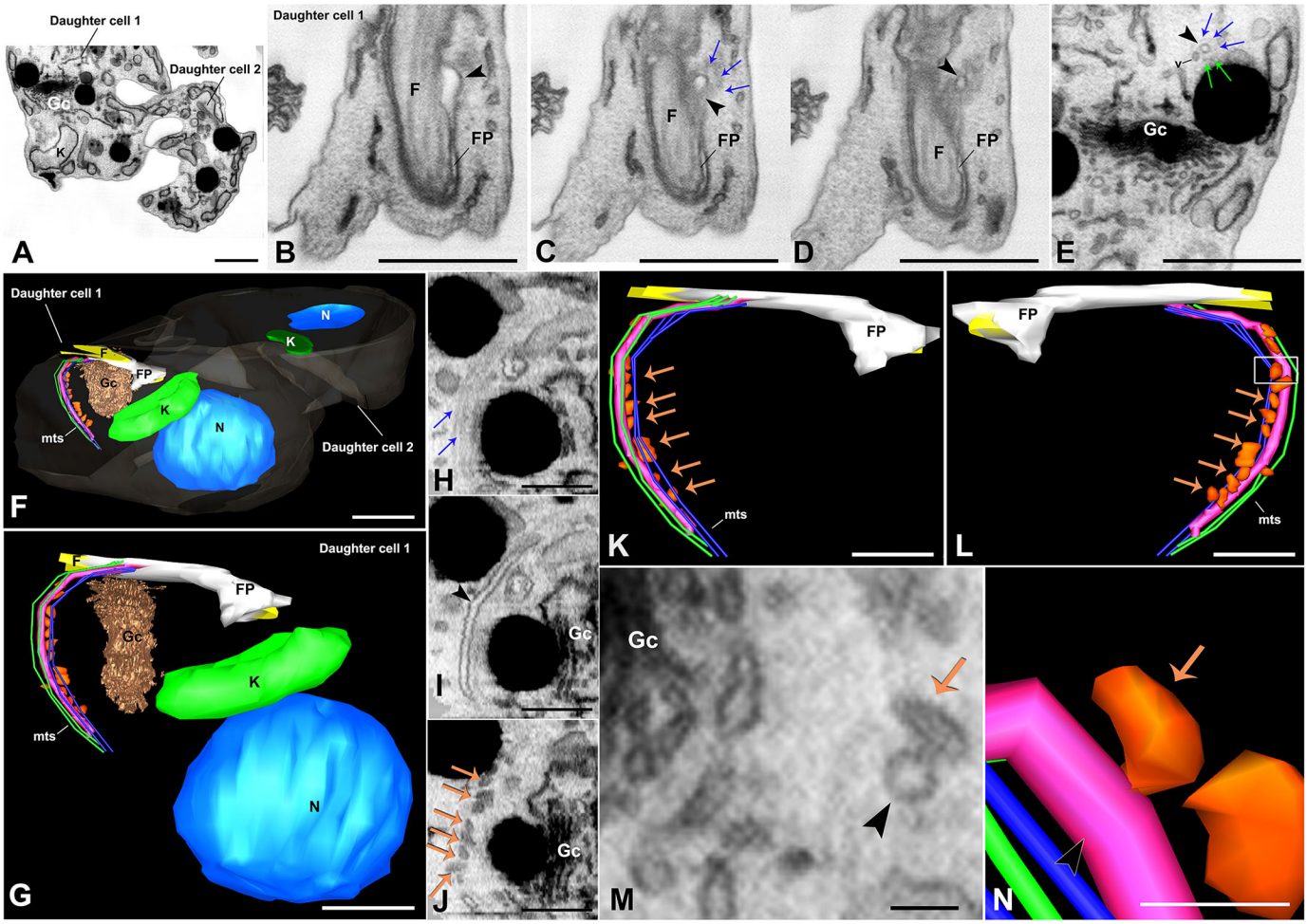

Fig. 7. The recently formed cytopharynx was already accompanied by vesicles. FIB-SEM images (A–E,H–J,M) and corresponding 3D model (F,G,K,L,N) of a *Trypanosoma cruzi* epimastigote in cytokinesis, showing a clearly identifiable (albeit short) cytopharynx in daughter cell 1 (the one on the left, in A; the flagellar pocket region of daughter cell 2 is not visible in this series). In the flagellar pocket (FP, in white) of daughter cell 1, a membrane invagination (arrowhead) that is accompanied by the cytopharynx microtubules (blue and green arrows in images, and blue and green tubes in 3D model) elongates into a bona fide cytopharynx (black arrowhead in images, and pink in 3D model). This structure bends near the Golgi complex (Gc, in gold) and extends towards the posterior of the cell, reaching the antero-posterior plane of the kinetoplast (K, in green). F, flagellum; v, vesicle. (H–J) Longitudinal sections of the cytopharynx in sequential *z* positions, showing the cytopharynx microtubules (blue arrows in H), the cytopharynx lumen with its typical electron-dense coat (arrowhead in I), and the vesicles (orange arrows) aligned to the microtubule-free side of the cytopharynx (J). (K,L) Detail of the 3D model showing the cytopharynx from different angles, to allow visualization of the microtubules (mts, blue and green tubes) on one side of the structure, and the vesicles (orange, orange arrows) on the opposite (microtubule-free) side. (M,N) In the microtubule-free side of the cytopharynx, corresponding to the rectangular area in L, a vesicle (orange arrow in M, and orange in N) is seen in direct contact with the cytopharynx membrane (black arrowhead). Scale bars: 1 µm (A–F); 0.5 µm (H–N). The complete imaging, by FIB-SEM, of the cell shown here can be found in Movie 4.

appears to occur ahead of cytopharynx elongation (Fig. 6). Overall, our data suggests that the microtubule quartet that accompanies the cytostome–cytopharynx complex in G1/S cells guides the formation of a new complex in each daughter cell during cytokinesis.

The cytopharynx quartet of microtubules physically connects the cytostome–cytopharynx complex to the flagellar pocket (Okuda et al., 1999; Alcantara et al., 2014). Although we did not observe cells at very early stages of flagellar pocket division, the presence of a MtQ lining the membrane of the each flagellar pocket in cells with duplicated and unsegregated kinetoplasts suggests that the formation of the new cytopharynx quartet occurs very early during flagellar pocket division. Kinetoplast segregation is intimately associated with flagellar pocket division, because these structures are linked by the tri-partite attachment complex (TAC), which connects the kinetoplast to the flagellar basal bodies (Ogbadoyi et al., 2003). Therefore, it is likely that the duplication of the short cytopharynx microtuble quartet is strictly coordinated with (and linked to) flagellar pocket division, and that this phenomenon ensures correct positioning of cytostome–cytopharynx complexes formed *de novo*, during cytokinesis.

The Golgi complex of *T. cruzi* epimastigotes is situated close to the flagellar pocket and the kinetoplast (Girard-Dias et al., 2012). As the cytostome–cytopharynx complex always bends around the Golgi complex, we suggested previously that the Golgi is the likely source of vesicles that fuse with the cytopharynx, to replace and maintain this differentiated membrane domain (Alcantara et al., 2014). The microtubule quartet of the cytopharynx was located in close proximity to the Golgi complex during the entire cell division process. Two additional microtubules that originated close to the base of the cytopharynx microtubule quartet, near the flagellar pocket membrane, were positioned at each side of the Golgi complex (Fig. 5H–J). These microtubules are ideally positioned to

Journal of Cell Science (2017) 130, 164-176 doi:10.1242/jcs.187419

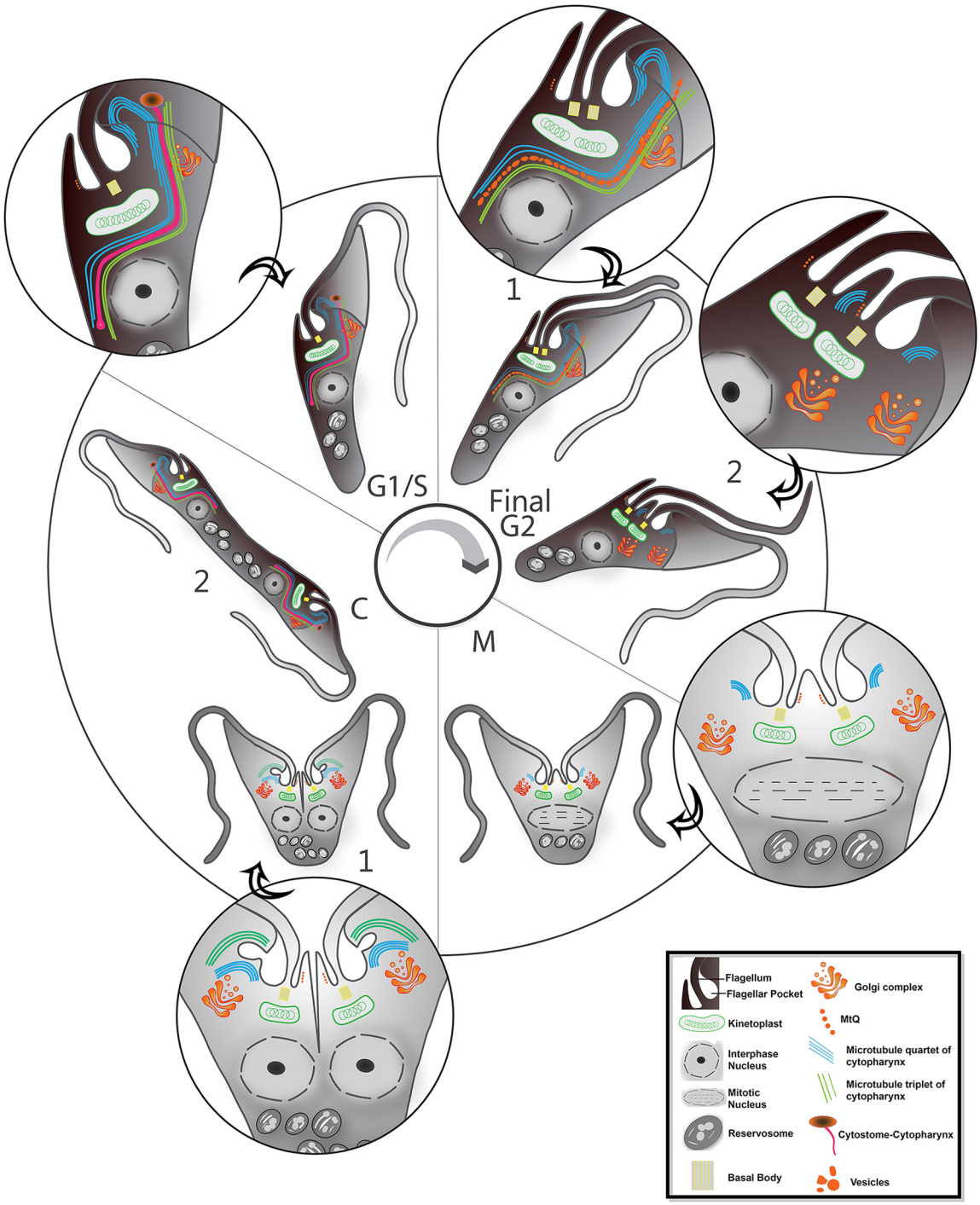

Fig. 8. Summarizing cartoon of the principal events affecting the cytostome–cytopharynx duplication during cell division. G1/S cells possess a helical-shaped cytostome–cytopharynx complex supported by two sets of microtubules: a quartet, which runs from the vicinity of the flagellar pocket membrane and a triplet, which originates just under the cytostome. At late G2, when the kinetoplast starts to divide (Final G2, 1), the cytostome–cytopharynx disassembles and many vesicles can be seen aligned to the cytopharynx microtubules. The microtubules maintain their normal disposition until the kinetoplast fully divides and two separated flagellar pockets are formed (Final G2, 2). At this stage, the microtubule triplet disappears and the cytopharynx microtubule quartet shortens, but is maintained in a short form close to the flagellar pocket membrane. The newly formed flagellar pocket is also associated with a short cytopharynx microtubule quartet and a new flagellar pocket MtQ. During M phase, the cytopharynx microtubule quartet remains in a short form until the beginning of cytokinesis (C, 1). At this stage, it starts to grow again and the microtubule triplet reappears. The new cytostome–cytopharynx complex is completed by a flagellar pocket membrane invagination that grows supported by the two sets of microtubules. At the end of cytokinesis (C2), when cells are still connected by their posterior end, fully formed cytostome–cytopharynx complexes are present, opening close to the flagellar pocket and extending deeply towards the cells posterior, assuming the typical helical shape supported by gutter-forming microtubules.

support vesicular movement in and out of the Golgi, and were also observed in epimastigotes in the G1 phase of the cell cycle (Alcantara et al., 2014). Similar cytoplasmic microtubules have been already identified in high-pressure-frozen *Leishmania mexicana* promastigotes (Weise et al., 2000), associated with the multivesicular tubule that represents the lysosomal compartment in

Journal of Cell Science (2017) 130, 164-176 doi:10.1242/jcs.187419

these parasites. Recently, an elegant paper associating fluorescent protein tagging and electron tomography to identify a flagellar attachment zone (FAZ) in *L. mexicana* (Wheeler et al., 2016) also found cytoplasmic microtubules originating in the flagellar pocket neighborhood. The authors suggest they might be the microtubules related to the lysosomal compartment. In *T. brucei*, the duplication of the Golgi complex is coordinated with that of the complex comprising the flagellum-flagellar pocket, basal bodies and kinetoplast during cell division (He et al., 2004), and is linked to the division of the bilobe, a cytoskeletal structure present near the flagellar pocket (He et al., 2005). In *T. cruzi*, no physical connections between the Golgi complex and the cytoskeleton have been reported to date. The individual cytoplasmic microtubules 1 and 2 observed here in dividing epimastigotes might represent this 'missing link' between the Golgi and the kinetoplast and flagellum-flagellar pocket structures, to help coordinate Golgi duplication and positioning with that of other anterior structures in the epimastigote cell. The function of the six different cytoplasmic microtubules in the flagellar pocket neighborhood in *T. cruzi* epimastigotes that we described previously (Alcantara et al., 2014), and their similarities with *T. brucei* and *L. mexicana* cytoplasmic microtubules, remains obscure.

The presence of numerous vesicles lining the path of the cytopharynx microtubules in late G2 cells that lack a cytostome–cytopharynx complex (Fig. 2) suggests that vesicle budding from the cytopharynx, in the absence of membrane renewal, might represent the mechanism of cytopharynx disassembly in late G2. However, we could not exclude the possibility that the vesicles observed lining the cytopharynx microtubules correspond to the typical vesicles that accompany the cytopharynx in G1/S cells, and that this structure is disassembled by an alternative mechanism. Our data strongly suggest that, during cytokinesis, each new cytostome–cytopharynx complex emerges as an invagination of the flagellar pocket membrane (near the flagellar pocket opening area), and that the cytostome opening is later displaced to the cell body surface, outside the pocket (Fig. 8), which might be concomitant with preoral ridge formation. Given the close proximity of the Golgi to the newly formed cytopharynx, and the presence of electron-dense vesicles aligned to this structure, we suggest that the fusion of Golgi-derived vesicles drives the elongation of the membrane domain of the cytopharynx, following the path of the quartet and triplet microtubules.

Finally, we demonstrated that the endocytic activity of cells in late G2, mitosis and beginning of cytokinesis was almost absent. This blockage in endocytosis was probably associated with the disassembly of the cytostome–cytopharynx complex, the main site for endocytosis in *T. cruzi* epimastigote forms (Porto-Carreiro et al., 2000). It is noticeable that we did not observe tracer uptake via the flagellar pocket while the cytostome was disassembled, which reinforces the diminished role of the flagellar pocket in the endocytic process of *T. cruzi* epimastigotes. In mammalian cells, endocytosis is also inhibited in cells undergoing mitosis and is resumed in anaphase (Jongsma et al., 2015). In these cells, the blockage seems to be related to an interruption in the fusion and fission processes involving endosomes. The endosomes would also donate membranes to the formation of the cleavage furrow. We do not have any data about the fate of the cytopharynx-derived membranes during cell division. They could contribute to the formation of the cleavage furrow or remain as vesicles, ready to fuse and form the cytopharynx again. However, our observation of the cytostome invagination beginning to form from the flagellar pocket membrane of the daughter cells suggests a different reassembly. The molecular mechanisms that govern endocytic pathway remodeling during cell division in *T. cruzi* and mammalian cells remain largely obscure.

Overall, our results identified the key events of the biogenesis of the cytostome–cytopharynx complex of *T. cruzi* epimastigotes, and showed that organelle assembly and disassembly mechanisms play a role in the trypanosomatid cell duplication cycle. The main findings regarding this process are summarized in Fig. 8.

The development of more reliable tools for the genetic manipulation of *T. cruzi*, as well as the identification of specific molecular markers for the cytopharynx, should improve our understanding of the molecular mechanisms that regulate assembly and disassembly of this important membrane domain during cell division.

MATERIALS AND METHODS

Parasites

Epimastigote forms of *Trypanosoma cruzi* clone Dm28c were cultivated in liver infusion tryptose (LIT) medium (Camargo, 1964) supplemented with 10% (v/v) heat-inactivated fetal calf serum (FCS) at 28°C. Three-day-old cultures were used in all experiments.

Cell cycle synchronization

To induce G1 arrest, epimastigotes (5×10^6 cells/ml) were incubated with 20 mM of hydroxyurea (HU), in LIT medium supplemented with 10% FCS, for 24 h at 28°C, as described previously (Galanti et al., 1994). After the HU block, parasites were washed extensively in LIT medium without HU and 'released' from cell cycle arrest in fresh medium supplemented with FCS. This moment was considered time 0 after HU block, and samples were removed for microscopy analysis hourly from 10 to 14 h post-release from HU block. At each time point (control, 1 h, and 10–14 h after HU release), cells were stained with DAPI (Sigma-Aldrich) and synchronization efficiency was evaluated by counting the cells (n=200) under the fluorescence microscope (Axio Observer, Zeiss).

Endocytosis assay

Holotransferrin bovine (Tf, Sigma Aldrich) was incubated with an excess of fluorescein isothiocyanate (FITC, Sigma Aldrich) in 0.1 M Na_2CO_3 buffer, pH 9.0, for 3 hours, at 4°C, under gentle shaking. After adding 50 mM NH_4Cl to quench free FITC, Tf–FITC was purified by gel filtration in a Sephadex G-25 column. The molar ratio of FITC to Tf was calculated using the absorbance at 280 nm (for Tf detection) and 495 nm (for FITC detection). Protein content was determined (RC-DC protein assay, BioRad) and 10 µg/ml Tf–FITC was used for parasite incubations.

Synchronized cells were submitted to endocytosis of Tf–FITC for 15 min at 28°C. The parasites were then fixed with 4% (v/v) paraformaldehyde in phosphate-buffered saline (PBS, pH 7.2), for 1 h. The cells were stained with DAPI, imaged and counted using a fluorescence microscope (Axio Observer, Zeiss).

Sample preparation for electron microscopy

Samples were fixed with 2.5% (v/v) glutaraldehyde in 0.1 M cacodylate buffer, pH 7.2, for 1 h at room temperature. Following a wash in cacodylate buffer, cells were post-fixed using an osmium-thiocarbohydrazide-osmium (OTO) protocol (Willingham and Rutherford, 1984). Briefly, cells were incubated in a post-fixative osmium solution containing 1% (v/v) osmium tetroxide, 0.8% (v/v) potassium ferrocyanide and 5 mM calcium chloride, in 0.1 M cacodylate buffer (pH 7.2), for 40 min, washed twice in water, and then incubated in a solution of 1% (w/v) thiocarbohydrazide (TCH, Sigma) in water, for 5 min. After three washes in water, cells were incubated again in the post-fixative osmium solution for 3 min. Following OTO post-fixation, samples were washed in water, dehydrated in an acetone series and embedded in epoxy resin (EMbed 812 Resin, EMS). The embedded material was observed by electron tomography and focused ion beam scanning electron microscopy (FIB-SEM), as described below.

Electron tomography

For electron tomography, 200-nm-thick serial sections of embedded samples were cut in a Leica EM UC7 ultramicrotome (Leica, Wetzlar, Germany), collected onto formvar-coated copper slot grids and stained with 5% (w/v) uranyl acetate and lead citrate. Then, 10-nm colloidal gold particles (Gold colloid, Sigma-Aldrich) were deposited onto both surfaces of the sections, to be used as fiducial markers during alignment of the tilted views. Single-axis tilt series (±60° with 1° increments) were produced from samples using the Xplore3D software, in a Tecnai-G^2 electron microscope (FEI Company, Eindhoven, Netherlands), operating at 200 kV, and coupled to a '4k×4k' pixel CCD camera. Alternatively, tomography was performed in a Tecnai Spirit electron microscope (FEI Company, Eindhoven, Netherlands) operating at 120 kV, and coupled to a '2k×2k' pixel CCD camera.

FIB-SEM

For observation by FIB-SEM, embedded samples were trimmed to a trapezium shape, and the block surface was smoothed by sectioning using a conventional diamond knife. The block was then glued to an SEM stub using carbon tape, with the smooth surface facing upwards, perpendicular to the microscope column. Samples were imaged using a Helios Nanolab 650 dual-beam microscope (FEI Company, Eindhoven, Netherlands) equipped with a gallium-ion source for focused-ion-beam milling, and a field-emission gun and an in-lens secondary electron detector for SEM imaging. The cross-sectional cut was made at ion beam currents of 2.5 nA and at an accelerating voltage of 30 kV. Back-scattered electron images were recorded at an accelerating voltage of 2 kV and a beam current of 0.8 nA, in the immersion lens mode, using a CBS (Concentric BackScatter) detector. A series of backscattered electron images were recorded in 'slice-and-view' mode, at a magnification of 15 K, with a pixel size of 8.9 nm and milling step size of 20 nm. After image capture, back-scattered electron images had their contrast inverted, to resemble conventional TEM images.

3D reconstructions and data analysis

Reconstructions and subsequent 3D data analyses were performed using the IMOD software package (Kremer et al., 1996). Tomogram generation (by R-weighted back-projection), joining of adjacent tomograms and FIB-SEM serial section alignment were performed using eTomo. Structures of interest in FIB-SEM and tomography images were manually segmented using 3DMOD, which was also used to produce 3D models.

Acknowledgements

We are grateful for the technical assistance of Luis Sergio Júnior (Inmetro, Rio de Janeiro, Brazil) and Thiago Luis de Barros Moreira (Centro Nacional de Bioimagem, Rio de Janeiro, Brazil), to Flavia F. Moreira Leite for critical reading of the manuscript and to Breno Alcantara for the beautiful drawing.

Competing interests

The authors declare no competing or financial interests.

Author contributions

C.L.A. and J.C.V. designed and performed experiments. W.S. and N.L.C.S. conceived and designed experiments and interpreted data. C.L.A. and N.L.C.S. wrote the paper. All authors commented on drafts of the paper.

Funding

This work was supported by Conselho Nacional de Desenvolvimento Científico e Tecnológico (CNPq) [grant number 472262/2012-2]; Coordenação de Aperfeiçoamento de Pessoal de Nível Superior (CAPES) scholarships to C.d.L.A. and J.C.V.; Financiadora de Estudos e Projetos (FINEP); and Programas Núcleos de Excelência (PRONEX) [grant number E-26/110.576/2010] and Cientista do Nosso Estado [grant number E-26/102.850/2012] from the Fundação Carlos Chagas Filho de Amparo à Pesquisa do Estado do Rio de Janeiro (FAPERJ).

Data availability

Movies 1–4 are hosted on FigShare: Movie 1, https://figshare.com/s/4f2a04bb1cdb6b0087be; Movie 2, https://figshare.com/s/5084667056ef0ef5e034; Movie 3, https://figshare.com/s/c2c535581ecee45d9d9a; Movie 4, https://figshare.com/s/16013f408be075258198.

Supplementary information

Supplementary information available online at http://jcs.biologists.org/lookup/doi/10.1242/jcs.187419.supplemental

References

Alcantara, C. L., Vidal, J. C., de Souza, W. and Cunha-e-Silva, N. L. (2014). The three-dimensional structure of the cytostome-cytopharynx complex of Trypanosoma cruzi epimastigotes. *J. Cell Sci.* **127**, 2227-2237.

Camargo, E. P. (1964). Growth and differentiation in Trypanosoma cruzi. I. Origin of metacyclic trypanosomes in liquid media. *Rev. Inst. Med. Trop. Sao Paulo* **6**, 93-100.

Cunha-e-Silva, N. L., Sant'Anna, C., Pereira, M. G. and de Souza, W. (2010). Endocytosis in Trypanosoma cruzi. *Open Parasitol. J.* **4**, 98-101.

De Souza, W. (2002). Basic cell biology of Trypanosoma cruzi. *Curr. Pharm. Des.* **8**, 269-285.

De Souza, W., Martinez-Palomo, A. and Gonzalez-Robles, A. (1978). The cell surface of Trypanosoma cruzi: cytochemistry and freeze-fracture. *J. Cell Sci.* **33**, 285-299.

Elias, M. C., da Cunha, J. P. C., de Faria, F. P., Mortara, R. A., Freymuller, E. and Schenkman, S. (2007). Morphological events during the Trypanosoma cruzi cell cycle. *Protist* **158**, 147-157.

Ferguson, M. L., Torri, A. F., Pérez-Morga, D., Ward, D. C. and Englund, P. T. (1994). Kinetoplast DNA replication: mechanistic differences between Trypanosoma brucei and Crithidia fasciculata. *J. Cell Biol.* **126**, 631-639.

Galanti, N., Dvorak, J. A., Grenet, J. and McDaniel, J. P. (1994). Hydroxyurea-induced synchrony of DNA replication in the Kinetoplastida. *Exp. Cell Res.* **214**, 225-230.

Girard-Dias, W., Alcântara, C. L., Cunha, E. S. N., de Souza, W. and Miranda, K. (2012). On the ultrastructural organization of Trypanosoma cruzi using cryopreparation methods and electron tomography. *Histochem. Cell Biol.* **138**, 821-831.

Guedes, P. M., Gutierrez, F. R. S., Silva, G. K., Dellalibera-Joviliano, R., Rodrigues, G. J., Bendhack, L. M., Rassi, A., Jr., Rassi, A., Schmidt, A., Maciel, B. C. et al. (2012). Deficient regulatory T cell activity and low frequency of IL-17-producing T cells correlate with the extent of cardiomyopathy in human Chagas' disease. *PLoS Negl. Trop. Dis.* **6**, e1630.

He, C. Y., Ho, H. H., Malsam, J., Chalouni, C., West, C. M., Ullu, E., Toomre, D. and Warren, G. (2004). Golgi duplication in Trypanosoma brucei. *J. Cell Biol.* **165**, 313-321.

He, C. Y., Pypaert, M. and Warren, G. (2005). Golgi duplication in Trypanosoma brucei requires Centrin2. *Science* **310**, 1196-1198.

Imoto, Y., Yoshida, Y., Yagisawa, F., Kuroiwa, H. and Kuroiwa, T. (2011). The cell cycle, including the mitotic cycle and organelle division cycles, as revealed by cytological observations. *J. Electron. Microsc.* **60** Suppl. 1, S117-S136.

Jensen, R. E. and Englund, P. T. (2012). Network news: the replication of kinetoplast DNA. *Ann. Rev. Microbiol.* **66**, 473-491.

Jongsma, M. L. M., Berlin, I. and Neefjes, J. (2015). On the move: organelle dynamics during mitosis. *Trends Cell Biol.* **25**, 112-124.

Kizilyaprak, C., Daraspe, J. and Humbel, B. M. (2014). Focused ion beam scanning electron microscopy in biology. *J. Microsc.* **254**, 109-114.

Kremer, J. R., Mastronarde, D. N. and McIntosh, J. R. (1996). Computer visualization of three-dimensional image data using IMOD. *J. Struct. Biol.* **116**, 71-76.

Lacomble, S., Vaughan, S., Gadelha, C., Morphew, M. K., Shaw, M. K., McIntosh, J. R. and Gull, K. (2009). Three-dimensional cellular architecture of the flagellar pocket and associated cytoskeleton in trypanosomes revealed by electron microscope tomography. *J. Cell Sci.* **122**, 1081-1090.

Lacomble, S., Vaughan, S., Gadelha, C., Morphew, M. K., Shaw, M. K., McIntosh, J. R. and Gull, K. (2010). Basal body movements orchestrate membrane organelle division and cell morphogenesis in Trypanosoma brucei. *J. Cell Sci.* **123**, 2884-2891.

Ogbadoyi, E. O., Robinson, D. R. and Gull, K. (2003). A high-order trans-membrane structural linkage is responsible for mitochondrial genome positioning and segregation by flagellar basal bodies in trypanosomes. *Mol. Biol. Cell* **14**, 1769-1779.

Okuda, K., Esteva, M., Segura, E. L. and Bijovsy, A. T. (1999). The cytostome of Trypanosoma cruzi epimastigotes is associated with the flagellar complex. *Exp. Parasitol.* **92**, 223-231.

Porto-Carreiro, I., Attias, M., Miranda, K., De Souza, W. and Cunha-e-Silva, N. (2000). Trypanosoma cruzi epimastigote endocytic pathway: cargo enters the cytostome and passes through an early endosomal network before storage in reservosomes. *Eur. J. Cell Biol.* **79**, 858-869.

Ramos, T. C. P., Freymüller-Haapalainen, E. and Schenkman, S. (2011). Three-dimensional reconstruction of Trypanosoma cruzi epimastigotes and organelle distribution along the cell division cycle. *Cytometry A J. Int. Soc. Anal. Cytol.* **79**, 538-544.

Robinson, D. R., Sherwin, T., Ploubidou, A., Byard, E. H. and Gull, K. (1995). Microtubule polarity and dynamics in the control of organelle positioning,

Journal of Cell Science (2017) 130, 164-176 doi:10.1242/jcs.187419

segregation, and cytokinesis in the trypanosome cell cycle. *J. Cell Biol.* **128**, 1163-1172.

Sherwin, T. and Gull, K. (1989). The cell division cycle of Trypanosoma brucei brucei: timing of event markers and cytoskeletal modulations. *Philos. Trans. R. Soc. Lond. B Biol. Sci.* **323**, 573-588.

Taylor, A. E. R. and Godfrey, D. G. (1969). A new organelle of bloodstream salivarian trypanosomes. *J. Protozool.* **16**, 466-470.

VataruNakamura, C., Ueda-Nakamura, T. and de Souza, W. (2005). Visualization of the cytostome in Trypanosoma cruzi by high resolution field emission scanning electron microscopy using secondary and backscattered electron imaging. *FEMS Microbiol. Lett.* **242**, 227-230.

Vaughan, S. and Gull, K. (2008). The structural mechanics of cell division in Trypanosoma brucei. *Biochem. Soc. Trans.* **36**, 421-424.

Vickerman, K. (1969). On the surface coat and flagellar adhesion in trypanosomes. *J. Cell Sci.* **5**, 163-193.

Webster, P. and Russell, D. G. (1993). The flagellar pocket of trypanosomatids. *Parasitol. Today* **9**, 201-206.

Weise, F., Stierhof, Y. D., Kühn, C., Wiese, M. and Overath, P. (2000). Distribution of GPI-anchored proteins in the protozoan parasite Leishmania, based on an improved ultrastructural description using high-pressure frozen cells. *J. Cell Sci.* **113**, 4587-4603.

Wheeler, R. J., Sunter, J. D. and Gull, K. (2016). Flagellar pocket restructuring through the Leishmania life cycle involves a discrete flagellum attachment zone. *J. Cell Sci.* **129**, 854-867.

Willingham, M. C. and Rutherford, A. V. (1984). The use of osmium-thiocarbohydrazide-osmium (OTO) and ferrocyanide-reduced osmium methods to enhance membrane contrast and preservation in cultured cells. *J. Histochem. Cytochem.* **32**, 455-460.

Woodward, R. and Gull, K. (1990). Timing of nuclear and kinetoplast DNA replication and early morphological events in the cell cycle of Trypanosoma brucei. *J. Cell Sci.* **95**, 49-57.